RSC Advances

PAPER

View Article Online
View Journal | View Issue

Cite this: *RSC Adv.*, 2017, **7**, 44547

Facet-dependent magnesiation behavior of α-Sn as an anode for magnesium ion batteries

Wei Jin and Zhiguo Wang *

Received 18th July 2017
Accepted 11th September 2017

DOI: 10.1039/c7ra07899d

rsc.li/rsc-advances

The adsorption and magnesiation behavior of Mg onto α-Sn and Mg_2Sn through (100), (110) and (111) surfaces were investigated by using first-principles calculations. It was found that the Mg atom prefers to be adsorbed on the surface rather than diffuse into the sub-surface of Sn. The diffusion energy barrier is higher for Mg diffusing from the surface to the subsurface compared with the internal diffusion. Mg diffuses much faster along the <100> direction than along the <110> and <111> directions. The diffusion process from the surface to the subsurface is a rate-limiting step for Mg intercalation into Sn. The surface magnesiation is also a rate-limiting step for Mg intercalation into Mg_2Sn though (100) and (110) surfaces, whereas the surface magnesiation of the Mg_2Sn (111) surface is easier than the (100) and (110) surfaces. Surface modification is necessary to improve the magnesiation behavior of Sn as an anode for MIBs, especially when the anode materials are reduced to the nanoscale.

1. Introduction

Magnesium ion batteries (MIBs) have attracted much attention in recent years[1–7] due to their advantages compared with current commercial lithium ion batteries, such as high safety, high specific capacity, and low price. To further improve the overall battery performance of MIBs, a variety of materials have been studied to be used as anodes and cathodes for MIBs.[8–10] Because of the incompatibility between Mg metal and conventional electrolyte, the development of the anode materials is slower than that of the cathode materials.[11] Among all the anode candidates, tin (Sn)[12,13] has been regarded as a promising anode for MIBs owing to its high capacity and compatibility with the conventional electrolyte. It was found that the Sn can endure much higher strain and capacity retention by reducing their size to nanoscale.[14,15] Many studies had been focus on the understanding of Mg diffusion process within the Sn anodes.[13,16] However, Mg ions transport in the Sn surface exposed to the electrolyte is of great importance as the first step of the Mg insertion into the anode. The surface magnesiation can hardly be observed by an experimental setup; density functional theory (DFT) calculations can provide an atomistic understanding of the magnesiation procedure and predict the electrochemical properties of surface magnesiation.[17,18] Kaghazchi *et al.*[18] have studied the lithiation of Li into Sn(100) surface and found that Li was more stable at interstitial sites between the topmost surface-layers of Sn(100) than at the surface sites and bulk sites using DFT. Jung *et al.*[19] investigated the intercalation of a Li atom into the surface and subsurface layers of Ge and Sn using DFT calculations. Their simulation results suggested that the rate-limiting step in Sn was the subsurface diffusion in both the Sn(100) and Sn(111) surfaces. They also found that Li diffused faster by at least two orders of magnitude along the [100] crystal orientation than along the [111] crystal orientation.[17]

Although Sn has been studied as anode for MIBs,[12,13] yet few studies have been performed on Mg magnesiation into Sn surfaces. As the surface lithiation is the rate-limiting step when Sn used as anode for lithium ion batteries, in this work we studied Mg magnesiation into Sn(100), Sn(110), Sn(111), Mg_2Sn(100), Mg_2Sn(110), and Mg_2Sn(111) surfaces using DFT calculations to understand the electrochemical behavior of the Sn as the anode materials for the MIBs.

2. Computational methods

All the calculations were carried out using the DFT as implemented within the SIESTA code.[20] The generalized gradient approximation (GGA) with Perdew–Burke–Ernzerhof (PBE) function was used to describe the electron exchange–correlation term.[21,22] The interactions between the core and valence electrons were described by nonlocal norm-conserving pseudopotentials.[23] The valence electron wave functions were expanded using double-ζ basis functions. For calculating the self-consistent Hamiltonian matrix elements, the charge density was projected on a real space grid with a cutoff of 150 Ry. The calculated bulk bond length of Sn–Sn was 2.89 Å for α-Sn, which was in good agreement with experimental value of 2.81 Å (ref. 24) and previous DFT calculated value of 2.88 Å.[19]

The surfaces of α-Sn were modeled using asymmetric slabs which composed of fourteen layers Sn atoms. One side of the

School of Physical Electronics, Center for Public Security Technology Research, University of Electronic Science and Technology of China, Chengdu, 610054, P. R. China. E-mail: zgwang@uestc.edu.cn

slabs was saturated with hydrogen atoms. The bottom four Sn atomic layers and the hydrogen layer were fixed to model the bulk Sn, and the remaining layers and the adsorbed Mg atom were allowed to relax freely. The slab thickness are 22.4, 31.8, and 25.5 Å for slabs with (100), (110) and (111) surfaces, respectively, which has been previously tested to be reliable[25] for investigating adsorption and diffusion for Li in Sn,[18,19] Ge[19] and Si[17,26] surfaces. The surfaces of the Mg_2Sn were modeled with slab thickness of 22.8, 32.3, and 25.3 Å for (100), (110) and (111) facets, respectively. The use of such asymmetric slabs was corrected by the dipole correction scheme of Neugebauer and Scheffler.[27] A vacuum spacing between the slabs and its image exceeds 20 Å to avoid the periodic image interactions.

Because the unreconstructed Sn(100)-(1 × 1) surface has been proved to be unstable,[18] we used the (4 × 2) surface unit cell to simulate the Sn(100) surface which is the ground state of Sn(100) consisting of buckled rows of Sn dimers, as shown in Fig. 1a. The relaxed Sn(110) and Sn(111) surfaces were shown in Fig. 1b and c, respectively. The adsorption energy (E_{ad}) of Mg on Sn surfaces was calculated using eqn (1):

$$E_{ad} = \frac{E_{Mg/slab} - nE_{Mg} - E_{slab}}{n} \quad (1)$$

where $E_{Mg/slab}$ and E_{slab} are the total energies of Sn slab with and without the Mg atom adsorption, respectively. E_{Mg} is the energy of a free Mg atom, and n is the number of adsorbed Mg atoms.

3. Results and discussion

3.1 Adsorption and magnesiation Mg into Sn(100) surface

There are four possible adsorption sites for Mg on Sn(100)-c (4 × 2) surface due to the symmetry of the geometric structure, shown in Fig. 1a. The H1 is the pedestal site, and B is the dimer bridge site. The cave (H2) site is located at the bottom of the trough and the valley bridge (T) site is on top of the third-layer Sn atom.[28] According to the definition of adsorption energy in eqn (1), a negative value means a favorable exothermic reaction between the substrate and Mg. The larger the negative value is, the more favorable of the reactions is. The calculated adsorption energies are listed in Table 1. Among all the adsorption sites, the H2 site is with the largest negative values, which means that the Mg prefers to be adsorbed at the H2 site. The H1 site is less stable than H2 site by 0.15 eV. The geometry optimizations for Mg adsorption starting from the B site eventually led to the stable H1 site. Besides, the T site is with adsorption energy of −0.53 eV, which is less stable adsorption site for Mg.

The energetically favorable adsorption site, H2, on Sn(100) was taken to be the initial site for the magnesiation of Mg into the Sn crystal through Sn(100) surface. Based on the adsorption energies listed in Table 1, the diffusion pathway H2 → S1 → S2 → S3 → S4 → S5 was investigated, which is the energetic favorable diffusion pathway for Mg magnesiation into Sn through (100) surface. A similar diffusion behavior was found for the lithiation of Si(100),[17,26] Sn(100)[18] and Ge (100)[19] surfaces. We used Sn (n = 1, 2, 3, 4, 5) to represent the adsorption sites of Mg at the nth layer of Sn away from the surface. As shown in Fig. 2, the Mg atom is energetically favorable at the tetrahedral site with the four nearest Sn atoms. Mg diffuses from on stable tetrahedral site to a nearest one by passing through a hexagonal site. The diffusion energy profile of Mg through the pathway H2 → S1 → S2 → S3 → S4 → S5 was shown in Fig. 2. The energy for Mg at the H2 and Sn site increases as the Mg magnesiation into the inside of Sn. The closer the adsorbed site to the Sn(100) surface, the lower the energy is, which is due to more effective stress release near the surface.[29] The diffusion energy barriers for Mg magnesiation into Sn through the (100) surface can be read from Fig. 2. The diffusion energy barrier is 1.05 eV for Mg diffuses from H2 to S1 site, and which are 0.84, 0.66, 0.65 and 0.63 eV for Mg diffuses to S2, S3, S4 and S5, respectively. It is can be seen that the surface magnesiation of Mg is with the highest diffusion energy barrier, whereas the inside diffusion with small one, which also shows less dependence on the position. So the surface magnesiation (H2 → S1) becomes the rate-limiting step during Mg intercalated into Sn through the (100) surface.

3.2 Adsorption and magnesiation Mg into Sn(110) surface

Three adsorption sites, *i.e.* H, B and T sites were considered for the adsorption of Mg on Sn(110) surface, as shown in Fig. 1b.

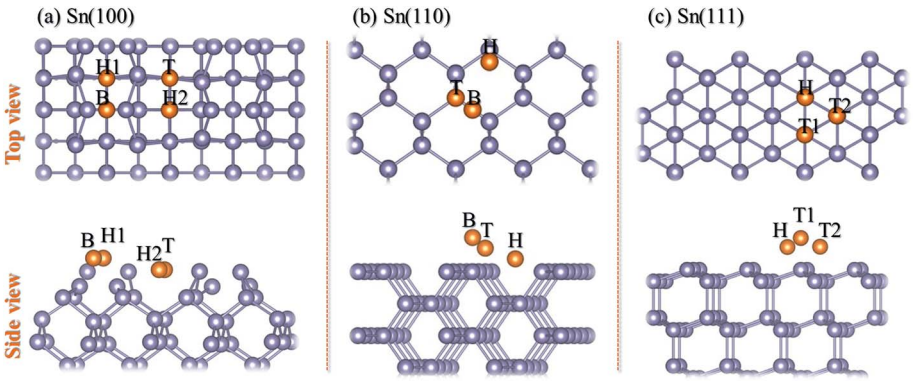

Fig. 1 Surface geometries and Mg adsorption sites of (a) Sn(100), (b) Sn(110) and (c) Sn(111), respectively. The orange balls represent the different adsorption sites (hollow sites, bridge sites and top sites are indicated by H, B, and T, respectively) on these surfaces, and gray balls represent Sn atoms.

Table 1 The adsorption energy of Mg atom on the Sn(100), Sn(110) and Sn(111) surfaces

Sn(100)		Sn(110)		Sn(111)	
Adsorption site	E_{ad}/eV	Adsorption site	E_{ad}/eV	Adsorption site	E_{ad}/eV
H1	−1.20	H	−4.39	H	−1.62
H2	−1.35	B	−1.39	T1	−0.81
B	−1.20	T	−1.39	T2	−1.46
T	−0.53				

The H site is above the center of triangle structure composed of three Sn atoms on the surface, B site is on top of a Sn–Sn bond, and T site is above the top of one Sn atom. The calculated adsorption energies were listed in Table 1. The H site is the energetically stable one with an adsorption energy of −4.39 eV. It was found that the T site is not stable for Mg adsorption, and the Mg atom moves from the T site to the adjacent H site after relaxation. The adsorption energy is −1.39 eV for the Mg adsorbed at B site, which is the metastable adsorption site.

The magnesiation of Mg into Sn through (110) surface were studied by investigating the diffusion of Mg along H → S1 → S2 → S3 → S4 → S5 diffusion path. The energetically stable sites for the intercalated Mg atom are the interstitial tetrahedral sites. The diffusion of Mg inside the Sn is through jumping from one tetrahedral site to an adjacent one by passing through a hexagonal site. The diffusion energy profile and diffusion paths for Mg magnesiation into Sn through (110) surface are shown in Fig. 3. The diffusion energy barrier for Mg diffusing along the H → S1 path is 1.58 eV, which is 0.44 eV higher than that for Mg along S1 → S2 path. The diffusion energy barriers are 1.09 eV, 0.69 and 0.74 eV for Mg diffuses along S2 → S3, S3 → S4 and S4 → S5 paths, respectively. It is like the diffusion of Mg through the (100) surface, and the H → S1 path is the rate-limiting step upon Mg intercalated into Sn through the (110) surface.

3.3 Adsorption and magnesiation Mg into Sn(111) surface

Three possible adsorption sites, *i.e.* H, T1 and T2 sites, were considered for the adsorption of Mg on the Sn(111) surface as shown in Fig. 1c. The H is above the center of hexagon structure composed of six non-plane Sn atoms. T1 and T2 sites are above the top of topmost and sub-high surface Sn atoms, respectively. The adsorption energies for Mg at H, T1, and T2 sites are listed in Table 1. The Mg prefers to occupy the H site on the Sn(111) surface with an adsorption energy of −1.62 eV. T2 site is less stable adsorption site, which is with an adsorption energy of 0.16 eV higher than the H site. The T1 site is not favorable adsorption site for Mg with the adsorption energy of −0.81 eV.

The magnesiation of Mg into Sn through the (111) surface was studied by considering the diffusion of Mg along the H → S1 → S2 → S3 → S4 → S5 path, and the diffusion energy

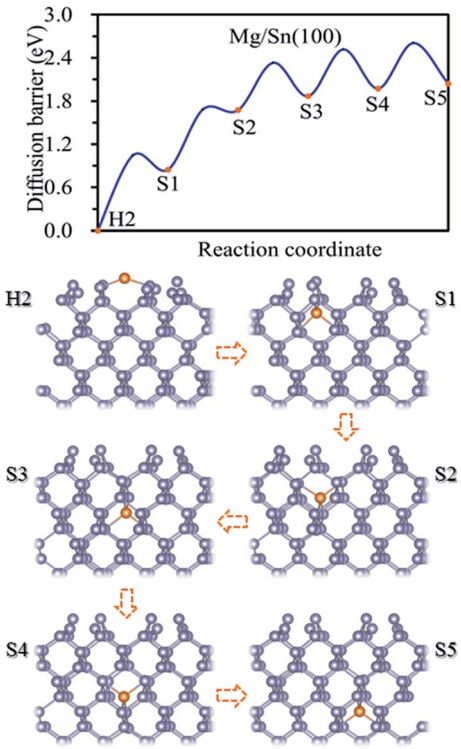

Fig. 2 Diffusion energy profile for Mg magnesiation into the surface and subsurface sites of Sn(100) and the atomic geometries at local minimum points in the profile.

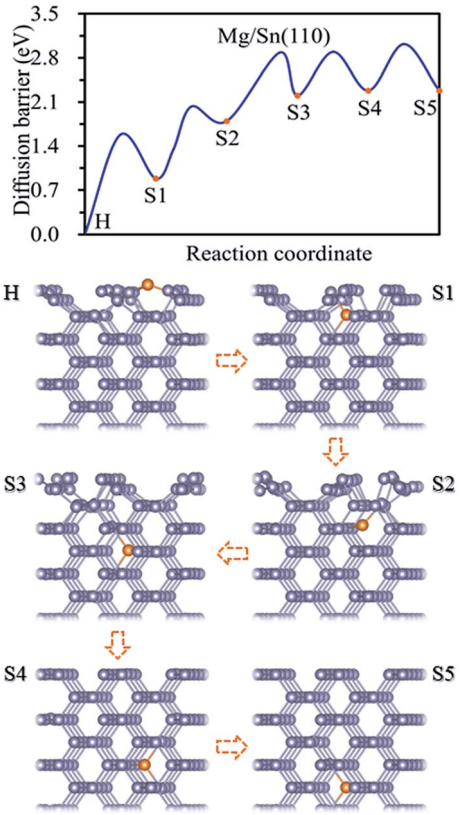

Fig. 3 Diffusion energy profile for Mg magnesiation into the surface and subsurface sites of Sn(110) and the atomic geometries at local minimum points in the profile.

profile was shown in Fig. 4. A similar diffusion behavior was found for Mg magnesiation into Sn through the (111) surface as through the (100) and (110) surfaces. The diffusion energy barrier is much higher for Mg diffuses from the surface to the subsurface of Sn, and the diffusion energy barrier is 1.27 eV for Mg along the H → S1 path. The diffusion barrier decreases as Mg diffuses inside the Sn. The diffusion energy barriers are 0.56 and 0.54 eV for Mg diffuses along S1 → S2 and S3 → S4 path, respectively. And they are 1.21 and 0.91 for Mg diffuses along S2 → S3 and S4 → S5 path, respectively. So the H → S1 path is the rate-limiting step upon Mg intercalated into Sn through the (111) surface. It is noticed that the diffusion of Mg inside the Sn through the (111) crystal facet with small and large diffusion energy barriers repeatedly. As shown in Fig. 4, the diffusion energy barriers of Mg diffuses are 0.56 eV (small) for S1 → S2, 1.21 eV (large) for S2 → S3, 0.54 eV (small) for S3 → S4, and 0.91 eV (large) for S4 → S5. The same diffusion behavior has been observed for Li diffusion into Si[17] and Sn[19] through the (111) surface. The diffusion of Mg inside the Sn is through jumping from one tetrahedral site to an adjacent one by passing through a hexagonal site. As the hexagon is perpendicular to the (111) surface, it is easy for the relaxation of atoms, which induces a small diffusion barrier. Whereas the hexagon is parallel to the (111) surface, it is difficult for the relaxation of atoms, which induces a large diffusion energy barrier. So a small and large diffusion energy barriers repeatedly when Mg diffuses along the S1 → S2 → S3 → S4 → S5 path.

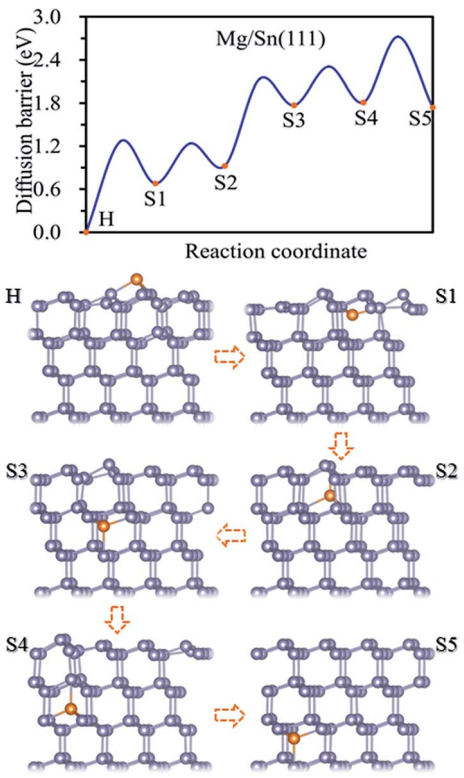

Fig. 4 Diffusion energy profile for Mg magnesiation into the surface and subsurface sites of Sn(111) and the atomic geometries at local minimum points in the profile.

3.4 Magnesiation of $Mg_2Sn(100)$, $Mg_2Sn(110)$ and $Mg_2Sn(111)$ surfaces

The crystalline Sn transforms to crystalline Mg_2Sn upon the insertion of Mg ions, and re-formation of crystalline Sn for the de-magnesiated crystalline Mg_2Sn,[12] we further studied the surface magnesiation behavior of (100), (110), and (111) surfaces for crystalline Mg_2Sn through a vacancy mechanism. Fig. 5a shows the diffusion energy profile for the magnesiation of $Mg_2Sn(100)$, $Mg_2Sn(110)$ and $Mg_2Sn(111)$ surfaces, and the corresponding diffusion paths (1 → 2 → 3 → 4 → 5 path) are shown in Fig. 5b, c, and d, respectively. Mg atom migrates from the Mg layer to the adjacent Mg layer by passing through an interstitial site located in the Sn layer through the $Mg_2Sn(100)$ surface. And the diffusion barriers are 1.15, 0.38, 0.48, and 0.47 eV for Mg diffuses from the outmost surface to the inside Mg layer along the 1 → 2 → 3 → 4 → 5 diffusion path through the $Mg_2Sn(100)$ surface. As Mg diffuses from one Mg–Sn layer to the adjacent Mg–Sn layer through $Mg_2Sn(110)$ surface, it needs to overcome energy barriers of 0.75, 0.42, 0.44, and 0.34 eV. The diffusion energy barriers are 0.20, 0.25, 0.36, and 0.42 eV for Mg diffuses into Mg_2Sn through (111) surface. It can be seen from Fig. 5a that the surface diffusion is a rate-limiting step upon Mg intercalated into Mg_2Sn through (100) and (110) surfaces, whereas the surface magnesiation of $Mg_2Sn(111)$ surface is easier than (100) and (110) surfaces.

From the above results, it can be seen that the diffusion energy barrier is higher for Mg diffuses from the surface to subsurface compared with the inside diffusion as Mg intercalated into Sn though (100), (110) and (111) surfaces and into Mg_2Sn through (100) and (110) surfaces. When Mg was intercalated into the Sn, the diffusion process from the surface to the subsurface is the rate-limiting step. Comparing the diffusion behavior of Mg into

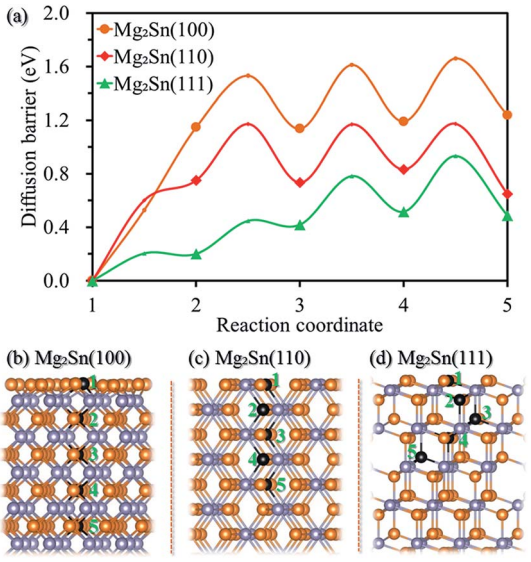

Fig. 5 (a) Diffusion energy profile for Mg magnesiation into Mg_2Sn though (100), (110) and (111) surfaces, along with the schematic diffusion path through (b) $Mg_2Sn(100)$, (c) $Mg_2Sn(110)$, and (d) $Mg_2Sn(111)$ surfaces. The orange and gray balls represent Mg atoms and Sn atoms, respectively. The black balls represent the Mg-vacancy.

Sn through (100), (110) and (111) surfaces, the one from the (100) surface is easier than (110) and (111) surfaces. The intercalation of Mg into Mg_2Sn through (111) surface is easier than through (100) and (110) surfaces. The surface magnesiation should be considered for Sn as anode for MIBs, especially when anode materials are decreased to nanoscale, and the surface electrochemical reaction is a key factor that affects battery performance. Surface modification such as metal doping[30] could be used to reduce the surface magnesiation barrier.

4. Conclusion

In conclusion, Mg magnesiation into α-Sn and Mg_2Sn through (100), (110) and (111) surfaces was investigated using density functional theory. The diffusion energies barriers are in the range 0.63–1.05, 0.68–1.58 and 0.54–1.27 eV for Mg diffuses in Sn along the <100>, <110> and <111> directions, respectively. Mg diffuses faster along the <100> direction than along <110> and <111> directions. The diffusion energy barriers are 1.05, 1.58 and 1.27 eV for Mg diffuses from the surface to subsurface by penetrating Sn(100), Sn(110) and Sn(111) surfaces, respectively, which are larger than the value of Mg diffuses inside Sn. The surface magnesiation is also the rate-limiting step upon Mg intercalated into Mg_2Sn though (100) and (110) surfaces. The Mg diffusion from the surface to subsurface becomes the rate-limiting step for Sn used as anode for MIBs. Surface modification to improve the magnesiation behavior should be considered for Sn as anode for MIBs, especially anode materials are decreased to nanoscale.

Conflicts of interest

There are no conflicts of interest to declare.

Acknowledgements

This work was financially supported by the National Natural Science Foundation of China (11474047) and the Fundamental Research Funds for the Central Universities (ZYGX2016J202). This work was carried out at National Supercomputer Center in Tianjin, and the calculations were performed on TianHe-1(A).

References

1 D. Aurbach, Y. Gofer, A. Schechter, O. Chusid, H. Gizbar, Y. Cohen, M. Moshkovich and R. Turgeman, *J. Power Sources*, 2001, **97**, 269–273.
2 Y. G. D. Aurbach, Z. Lu, A. Schechter, O. Chusid, H. Gizbar, Y. Cohen, V. Ashkenazi, M. Moshkovich, R. Turgeman and E. Levi, *J. Power Sources*, 2001, **97**, 28–32.
3 M. M. Huie, D. C. Bock, E. S. Takeuchi, A. C. Marschilok and K. J. Takeuchi, *Coord. Chem. Rev.*, 2015, **287**, 15–27.
4 J. S. Kim, W. S. Chang, R. H. Kim, D. Y. Kim, D. W. Han, K. H. Lee, S. S. Lee and S. G. Doo, *J. Power Sources*, 2015, **273**, 210–215.
5 E. Levi, Y. Gofer and D. Aurbach, *Chem. Mater.*, 2010, **22**, 860–868.
6 H. D. Yoo, I. Shterenberg, Y. Gofer, G. Gershinsky, N. Pour and D. Aurbach, *Energy Environ. Sci.*, 2013, **6**, 2265–2279.
7 S. Rasul, S. Suzuki, S. Yamaguchi and M. Miyayama, *Electrochim. Acta*, 2013, **110**, 247–252.
8 Y. L. Liang, R. J. Feng, S. Q. Yang, H. Ma, J. Liang and J. Chen, *Adv. Mater.*, 2011, **23**, 640–644.
9 C. Ling, R. Zhang, T. S. Arthur and F. Mizuno, *Chem. Mater.*, 2015, **27**, 5799–5807.
10 W. Jin, Z. Wang and Y. Q. Fu, *J. Mater. Sci.*, 2016, **51**, 7355–7360.
11 D. L. Aurbach, Z. Lu, A. Schechter, Y. Gofer, H. Gizbar, R. Turgeman, Y. Cohen, M. Moshkovich and E. Levi, *Nature*, 2000, **407**, 724–727.
12 N. Singh, T. S. Arthur, C. Ling, M. Matsui and F. Mizuno, *Chem. Commun.*, 2013, **49**, 149–151.
13 Z. Wang, Q. Su, J. Shi, H. Deng, G. Q. Yin, J. Guan, M. P. Wu, Y. L. Zhou, H. L. Lou and Y. Q. Fu, *ACS Appl. Mater. Interfaces*, 2014, **6**, 6786–6789.
14 Y. H. Xu, Q. Liu, Y. J. Zhu, Y. H. Liu, A. Langrock, M. R. Zachariah and C. S. Wang, *Nano Lett.*, 2013, **13**, 470–474.
15 J. Chen and F. Y. Cheng, *Acc. Chem. Res.*, 2009, **42**, 713–723.
16 O. I. Malyi, T. L. Tan and S. Manzhos, *J. Power Sources*, 2013, **233**, 341–345.
17 S. C. Jung and Y. K. Han, *Phys. Chem. Chem. Phys.*, 2011, **13**, 21282–21287.
18 P. Kaghazchi, *J. Chem. Phys.*, 2013, **138**, 054706.
19 S. C. Jung and Y. K. Han, *Phys. Chem. Chem. Phys.*, 2013, **15**, 13586–13592.
20 T. Slusarski, B. Brzostowski, D. Tomecka and G. Kamieniarz, *Acta Phys. Pol., A*, 2010, **118**, 967–968.
21 G. Kresse and J. Furthmuller, *Comput. Mater. Sci.*, 1996, **6**, 15–50.
22 G. Kresse and D. Joubert, *Phys. Rev. B: Condens. Matter Mater. Phys.*, 1999, **59**, 1758–1775.
23 N. Troullier and J. L. Martins, *Phys. Rev. B: Condens. Matter Mater. Phys.*, 1991, **43**, 8861–8869.
24 C. Kittel, *Introduction to Solid State Physics*, New York, 2005.
25 V. Fiorentini and M. Methfessel, *J. Phys.: Condens. Matter*, 1996, **8**, 6525–6529.
26 B. Peng, F. Cheng, Z. Tao and J. Chen, *J. Chem. Phys.*, 2010, **133**, 034701.
27 J. Neugebauer and M. Scheffler, *Phys. Rev. B: Condens. Matter Mater. Phys.*, 1992, **46**, 16067–16080.
28 Y. Morikawa, K. Kobayashi and K. Terakura, *Surf. Sci.*, 1993, **283**, 377–382.
29 T. L. Chan and J. R. Chelikowsky, *Nano Lett.*, 2010, **10**, 821–825.
30 B. R. Long, M. K. Y. Chan, J. P. Greeley and A. A. Gewirth, *J. Phys. Chem. C*, 2011, **115**, 18916–18921.